Journal of Aerosol Science 171 (2023) 106159

Contents lists available at ScienceDirect

Journal of Aerosol Science

journal homepage: www.elsevier.com/locate/jaerosci

Photochemical transformation and secondary aerosol formation potential of Euro6 gasoline and diesel passenger car exhaust emissions

Anni H. Hartikainen [a], Mika Ihalainen [a], Pasi Yli-Pirilä [a], Liqing Hao [b], Miika Kortelainen [a], Simone M. Pieber [c,d], Olli Sippula [a,e,*]

[a] Department of Environmental and Biological Sciences, University of Eastern Finland, P.O. Box 1627, 70211, Kuopio, Finland
[b] Department of Technical Physics, University of Eastern Finland, P.O. Box 1627, 70211, Kuopio, Finland
[c] Empa – Swiss Federal Laboratories for Materials Science and Technology, Laboratory for Air Pollution/Environmental Technology, 8600, Dübendorf, Switzerland
[d] AirUCI (Atmospheric Integrated Research), University of California, CA, 92697-2025, Irvine, USA
[e] Department of Chemistry, University of Eastern Finland, P.O. Box 111, 80101, Joensuu, Finland

ARTICLE INFO

Keywords:
Secondary aerosol
Photochemistry
Passenger vehicles
Particulate matter
Urban air
Environmental chamber

ABSTRACT

Traffic remains a major source of urban air pollution although emission regulations have led to significant reductions in exhaust emissions of new vehicles. In this work the photochemical transformation of exhaust emissions from gasoline and diesel passenger vehicles compliant with the current European 'Euro6' emission standard and operated with traditional and alternative fuels was investigated using an environmental chamber. By assessing four different engine operation conditions, we show that vehicle operation notably affects the exhaust composition and secondary aerosol formation potential. For the gasoline vehicle, secondary aerosols dominate the total particulate emissions. In contrast, we observe no substantial secondary aerosol formation for exhaust emissions of a Euro6-level diesel vehicle. High engine load operation and cold start of the gasoline vehicle led to 11–470-fold particulate mass enhancement, while for moderate driving conditions the enhancement ratio was below 2. High aerosol enhancements also led to strong increases in particle light absorption. The results underline the necessity for future directives to include the emission components leading to secondary pollution, in addition to the freshly emitted pollutants. The link observed between secondary organic aerosol (SOA) formation and gaseous aromatic hydrocarbon emissions suggests that monitoring and limiting these gaseous species can provide an indirect regulation for SOA. Additionally, ammonia released as a byproduct of the gasoline vehicle is confirmed as an important precursor for secondary aerosols.

1. Introduction

Traffic is a major source of urban air particulate matter (PM) and gaseous pollution. The harmful effects of air pollution have been abated by introduction of increasingly tightening regulations on gaseous and particle emissions of passenger vehicles(Hooftman et al.,

* Corresponding author. Department of Environmental and Biological Sciences, University of Eastern Finland, P.O. Box 1627, 70211, Kuopio, Finland.
E-mail address: olli.sippula@uef.fi (O. Sippula).

https://doi.org/10.1016/j.jaerosci.2023.106159
Received 9 December 2022; Received in revised form 15 February 2023; Accepted 26 February 2023
Available online 10 March 2023

2018; Wu et al., 2017). To comply with current emission regulations, gasoline exhaust gases are normally cleaned by three-way catalysts (TWCs). The use of gasoline particulate filters (GPFs) for the reduction of particulate emissions is also becoming increasingly popular. In modern diesel vehicles, nitrogen oxide (NO_x) emissions are reduced using selective catalytic reduction (SCR), carbon monoxide (CO) and hydrocarbons (HC) by diesel oxidation catalysts (DOCs), and PM emissions by diesel particle filters (DPFs) (Suarez-Bertoa et al., 2020). The emissions from vehicles compliant with the currently enforced emission limits can be considered low in comparison to emissions from older vehicles. Since 2015, European passenger vehicles need to comply with so-called Euro6-level regulations, which are roughly equivalent to US Tier 3 or China 6 standards. However, certain driving conditions lead to momentarily high pollutant concentrations. Exhaust emissions are typically high during cold start, when temperatures are low in the engine and in the exhaust after-treatment system(Karjalainen et al., 2016; Kostenidou et al., 2021; Kuittinen, McCaffery, Peng, et al., 2021; Park et al., 2021; Saliba et al., 2017). Additionally, vehicular emissions are significantly increased in high engine power conditions, such as during acceleration or driving uphill and at high speeds (Kostenidou et al., 2021; Kuittinen, McCaffery, Peng, et al., 2021; Saliba et al., 2017; Yang et al., 2020).

Once emitted, gaseous and particulate compounds are further altered by various atmospheric processes, including oxidation and functionalization by hydroxyl (OH) and nitrate (NO_3) radicals, ozone (O_3), and photolysis(Heald & Kroll, 2020). These oxidation processes lead to the formation of secondary PM in the atmosphere, including secondary organic aerosol (SOA) and secondary inorganic aerosol (SIA). The contribution of engine exhausts to urban air secondary aerosols has been studied by several different methodologies, including ambient air studies and well-defined laboratory experiments in environmental chambers, where the transformation of the sample can be simulated at close to realistic atmospheric conditions, and oxidative flow reactors (OFRs), that generally provide higher time resolution for the measurements of exhaust emission secondary aerosol formation potential(Chirico et al., 2010; Karjalainen et al., 2016; Kuittinen, McCaffery, Peng, et al., 2021; Pieber et al., 2018; Timonen et al., 2017; Tkacik et al., 2014). The previous studies highlight that the majority of PM emissions from passenger vehicles may be associated with secondary formation. Aromatic hydrocarbons (ArHCs) have been identified as the major organic gaseous compounds (OGCs) acting as SOA precursors in vehicular exhaust. For gasoline vehicles, SOA formation has been strongly linked with the aromatic content in fuel and exhaust(Kuittinen, McCaffery, Zimmerman, et al., 2021; Peng et al., 2017; Pieber et al., 2018; Timonen et al., 2017). For diesel vehicles, comparatively higher amount of fuel-derived SOA has been estimated to be formed by aliphatic precursors(Gentner et al., 2017). In addition, organic emissions originating from motor lubrication oil, present often as long chain alkanes, can play an important role in SOA formation for both diesel and gasoline exhausts (Canagaratna et al., 2010; Gentner et al., 2017; Zhao et al., 2017). Furthermore, inorganic emissions, such as SO_2, NO_x and NH_3, may lead to SIA formation. Notable potential for SIA formation has been reported for modern gasoline direct injection (GDI) vehicle exhaust, particularly when vehicles are operated under high power or during acceleration events(Karjalainen et al., 2016; Kuittinen, McCaffery, Peng, et al., 2021; Link et al., 2017; Roth et al., 2020). This has been linked with TWCs, which emit NH_3 as a byproduct especially under fuel-rich driving conditions(Mejía-Centeno et al., 2007). On the other hand, in diesel vehicles, SCR systems utilizing ammonia for NO_x reduction can lead to NH_3 emissions, and specific NH_3 slip catalysts have been developed to counteract this problem(Guan et al., 2014; Suarez-Bertoa et al., 2020). Consequently, development of vehicle technology and emission after-treatment techniques may notably alter the influence of passenger vehicles to secondary aerosol formation in ambient air. There is currently a clear lack of data on exhaust emission secondary aerosol potentials from the Euro6-compliant modern vehicles. Further, there is a particular lack of secondary aerosol emission data concerning cold start and prolonged high engine load conditions (e.g. uphill driving, high speed driving at highway), which are not represented in standardized test cycles but may lead to specifically high secondary aerosol formation potential (e.g. Karjalainen et al., 2016; Kuittinen, McCaffery, Peng, et al., 2021; Link et al., 2017; Timonen et al., 2017).

In this work, we investigated the photochemical transformation of emissions from Euro6-level gasoline and diesel passenger vehicles in an environmental chamber. The main objective was to determine emission factors for secondary aerosol formation potential under different driving conditions, particularly including cold start and high engine load conditions, and with different fuel reformulations. Further, we aimed to clarify the usefulness of ArHC emissions as a proxy for SOA formation potential of Euro6-level passenger vehicles. Finally, we evaluated the impact of photochemical atmospheric processes on the emission characteristics, including particulate compositions and aerosol optical properties.

2. Materials and methods

2.1. Vehicle operation, fuels, and sampling

Experiments were conducted in the ILMARI combustion laboratory of the University of Eastern Finland (www.uef.fi/ilmari) using Euro6-level rated passenger vehicles: a SEAT Arona EURO6b gasoline engine car equipped with a three-way catalytic converter and a SEAT Ateca EURO 6d-temp diesel engine car equipped with an oxidizing catalytic converter, a DPF and an SCR. The experimental setup is illustrated in Supplemental Figure S1.

The vehicles were operated by a chassis dynamometer (Rototest VPA-RX3 2WD) and run under four different conditions. The driving conditions were 1) cold start and subsequent cruising at 70 km h^{-1} (CSC70), 2) driving at 120 km h^{-1} resembling typical highway conditions (D120), 3) high engine load operation with an engine speed of 3000 rpm and a wheel power of approximately 40 kW (WP40 kW), and 4) at an engine speed of 5000 rpm and a wheel power of approximately 50 kW (WP50kW).

The engine conditions in D120 and WP40 kW resemble uphill driving scenarios, where the engine speed and the wheel power were identical for the two vehicles. However, due to differences between the cars (transmission, mass, drag), the reached velocity and representative hill steepness were different. Namely, D120 represents a 12% or a 6% hill climb for the gasoline and diesel vehicle,

respectively, whereas WP40 kW represents a 12% hill climb at 67 km h^{-1} or a 6% hill climb at 80 km h^{-1} for the gasoline and diesel vehicle, respectively. WP50kW is an engine condition typical for transient acceleration phases of class 3 modern cars in WLTP test cycle. This setting was used only with the gasoline vehicle, for which it represents driving at 67 km h^{-1} velocity and extra load equaling to 1.6 m s^{-2} acceleration. As a steady state the driving condition for the used vehicle represents high velocity driving at 157 km h^{-1} velocity.

In the cold start experiments, the sampling to the chamber was started at the same time with the engine start, and stable velocity was reached within 15 s from the start of the engine. The engine rested for at least 12 h before the cold start experiments. In the other experiments, the engine was first warmed up at 3000 rpm and with 50 Nm load for 5 min, after which the driving parameters were changed to those used in the experiment, and the engine was stabilized another 5 min before starting the sample input. The stabilization was closely monitored by following the engine temperature and the primary emission concentrations in the exhaust gas. Further information for the driving conditions is given in Table S1.

The diesel fuels used were 7% renewable biodiesel (B7) and 100% hydrotreated vegetable oil fuel (HVO). The gasoline fuels used were commercially available ethanol-blend gasoline fuels (E5 and E10) and a reformulated gasoline fuel (RFG) with an alcohol content of approximately 20%. Fuel changes were performed in an official workshop, where the fuel tank was emptied and cleaned between the experiments on different fuels. Primary NO, CO, and CO_2 concentrations were measured at the tailpipe by single gas analyzers (Siemens), and the total gaseous hydrocarbon (THC) content was measured by a flame ionization detector (FID, Siemens). The gaseous primary emissions were monitored by a Fourier transform infrared multicomponent gas analyzer (FTIR, Gasmet DX4000). A partial flow of exhaust was sampled, prediluted and subsequently fed into an environmental chamber using a combination of a porous tube diluter and an ejector diluter (Venacontra, Finland). The dilution was done using room-temperature air and controlled using CO_2 as a marker gas. The particle number in the diluted fresh exhaust was measured by a Fast Mobility Particle Sizer (FMPS, TSI Model 3091).

2.2. Aging procedure in the environmental chamber

A 29 m^3 Teflon environmental chamber (Leskinen et al., 2015) was operated in batch mode at a relative humidity of 55 ± 5% and at an ambient temperature of 23 ± 2 °C. A 20 min stabilization period after sample injection allowed for mixing within the chamber and analysis of the primary sample composition. After stabilization, 20–25 ppb of butanol-*d9* was added to quantify the hydroxyl radical (OH) exposure during subsequent atmospheric aging(Barmet et al., 2012). Hydrogen peroxide (H_2O_2) was added as a precursor for OH radicals by passing clean air over 0.5 mL of H_2O_2 in a 30% H_2O solution. THC/NO ratios in the fresh diesel exhaust were below 0.4 ppm C/ppm (Table S2), and atmospherically representative OGC/NO_x ratios of 5 ppm C/ppm were reached by the addition of propene to the chamber in the diesel vehicle experiments. For gasoline vehicle experiments, addition of propene was not required as the THC/NO ratios in the fresh exhaust ranged 2–14 ppm C/ppm (Table S2), which are representative for typical urban air conditions. The emission mixture was then photochemically aged for 4 h in the chamber under UV blacklights centered at a wavelength of 340 nm. The OH exposures and the atmospheric equivalent ages as atmospheric equivalent hours (eqv.h; at ambient average OH mixing ratio 10^6 cm^{-3}) at the end of each experiment are given in Table S3.

Particulate wall losses were determined to be 0.001 min^{-1} based on the decay of particulate mass in conditions where no formation of new particulate mass or loss of, e.g., secondary NH_4NO_3 is expected.(Hao et al., 2011). The fates of the low-volatility organic compounds (LVOCs) capable of irreversible condensation were assessed as provided in Supplementary Section S-2(Palm et al., 2016). Absolute LVOC wall losses were at their minimum (2×10^{-4} s^{-1}) directly after filling volume of the chamber. However, the relative share of wall loss as LVOC fate decreased upon aging due to the increase in particulate condensation sink ($CS_{PM,}$ Figure S2). Overall, during the gasoline-engine experiments, more than 96% of LVOCs were estimated to have condensed onto the particles. For most of the diesel-engine experiments, over 40% of the LVOCs remained in the gas phase due to the low CS_{PM}, while wall losses accounted for approximately 10% of the LVOC fate by the end of experiment (Figures S3-S4). In these experiments, due to the low CS_{PM}s only a fraction (23–77%) of the condensable organic species exists in the particulate phase, which constrains the quantification of secondary aerosol emission factors of the diesel vehicle.

2.3. Aerosol measurements from the chamber

The composition of submicron PM was measured with a high-resolution soot particle aerosol mass time-of-flight spectrometer (SP-AMS, Aerodyne Research Inc). Studied PM fractions included nonrefractory PM (organic aerosol (OA), NO_3, SO_4, and NH_4) and refractory light-absorbing PM, namely, refractory black carbon (rBC). In addition, the elemental composition of OA was analyzed, including the determination of average organic carbon oxidation state ($\overline{OS_C}$). Technical details of SP-AMS use are available in Supplementary Section S-3.

The particle concentration and size distribution in the chamber were measured by two scanning mobility particle sizers (SMPS, Model 3080, TSI): "long-SMPS" (DMA 3081, TSI) and "nano-SMPS" (DMA 3085, TSI), which were used to measure particle sizes in the range of 14–661 nm and 2–64 nm, respectively. SMPS data were used to evaluate the evolution of particle size distributions (Figure S5) and CS_{PM} during the aging process, and for calculation of the geometric mean mobility diameter (GMD) and geometric standard deviation (GSD) in the unimodal size distributions. PM mass concentrations were calculated from the long-SMPS size distributions using estimated particle densities based on the aerosol composition measured by SP-AMS and chemical component-specific density estimations as described in the Supplementary Section S-4.

PM light absorption was measured by using a seven-wavelength aethalometer (AE33, Magee Scientific). Optically derived

equivalent black carbon (eBC) mass was calculated assuming a default mass absorption coefficient of 7.77 $m^2\ g^{-1}$ for infrared (IR) absorption at 880 nm. The absorption Ångström exponents (AAEs) for the aerosol were determined based on absorption measurements at wavelengths of 470 nm and 950 nm. These optical parameters were used to examine the changes in aerosol light absorption in relation to photochemical aging.

Organic gaseous compounds (OGCs) were identified and quantified by a proton transfer reactor time-of-flight mass spectrometer (PTR-ToF-MS; PTR-TOF 8000, Ionicon Analytik, Innsbruck, Austria)(Jordan et al., 2009) operated with H_3O^+ as the primary ion; see Supplementary Section S3 for technical details. The compound detection limit was set at three times the standard deviation when measuring the chamber background.

OH exposure was assessed by online tracing of butanol-d9 by PTR-ToF-MS (Barmet et al., 2012). PTR-ToF-MS was not available for the RFG experiments, for which the decay in butanol-d9 was assessed based on TD-GC–MS (TD: ATD400 Automatic Thermal Desorption system, PerkinElmer, USA; GC–MS: GC 6890, MSD 5973, Hewlett-Packard, USA) measurements on desorption tubes (Tenax TA/Carbograph 5TD, 200 mL/min, 15 min). TD-GC–MS samples were collected at the beginning and end of each experiment, and linear exposure in the chamber was then assumed. O_3, NO, NO_2, and SO_2 in the chamber were measured continuously in ppb level by an UV photometric O_3 analyzer (49i, Thermo Fisher Scientific Inc., MA, USA), a chemiluminescent NO_x gas analyzer (42i, Thermo Fisher Scientific Inc., MA, USA), and a pulsed fluorescence SO_2 gas analyzer (43i, Thermo Fisher Scientific Inc., MA, USA).

3. Results and discussion

Emission factors (EFs) in the fresh and aged exhaust are presented in Figs. 1 and 2. Numeric values are available in Table S2 for fresh exhaust and in Table S3 at OH exposure equivalent to 24 h of exposure in ambient air (0.86×10^{11} molec. cm^{-3}) and at the end of the aging experiment.

3.1. Primary emissions from the diesel vehicle

For the diesel vehicle, SMPS-based EFs of primary particulate mass were below 0.01 mg km^{-1}, while the number of particles larger

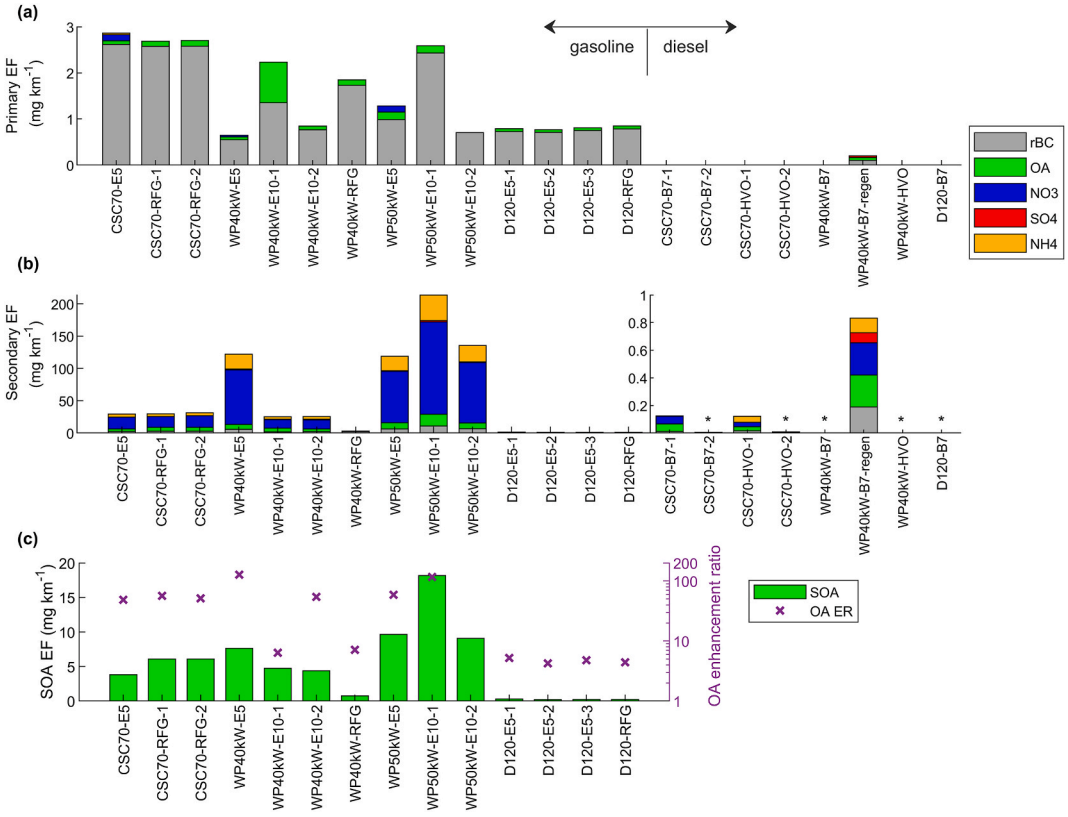

Fig. 1. Particulate emission factors, measured by SP-AMS, for the fresh (a) and aged exhausts at 24 h of atmospheric equivalent photochemical exposure (b), and the EFs of secondary organic aerosol (SOA) together with the enhancement ratios (ER) of OA, i.e., the ratio of total OA at the end of experiment to the primary (P) OA (in logarithmic scale) (c). SOA ER in WP50kW-10-2 cannot be determined due to POA emissions below detection limit (below 0.09 mg km^{-1}). *in these diesel experiments, secondary EFs were below detection limits. (For interpretation of the references to color in this figure legend, the reader is referred to the Web version of this article.)

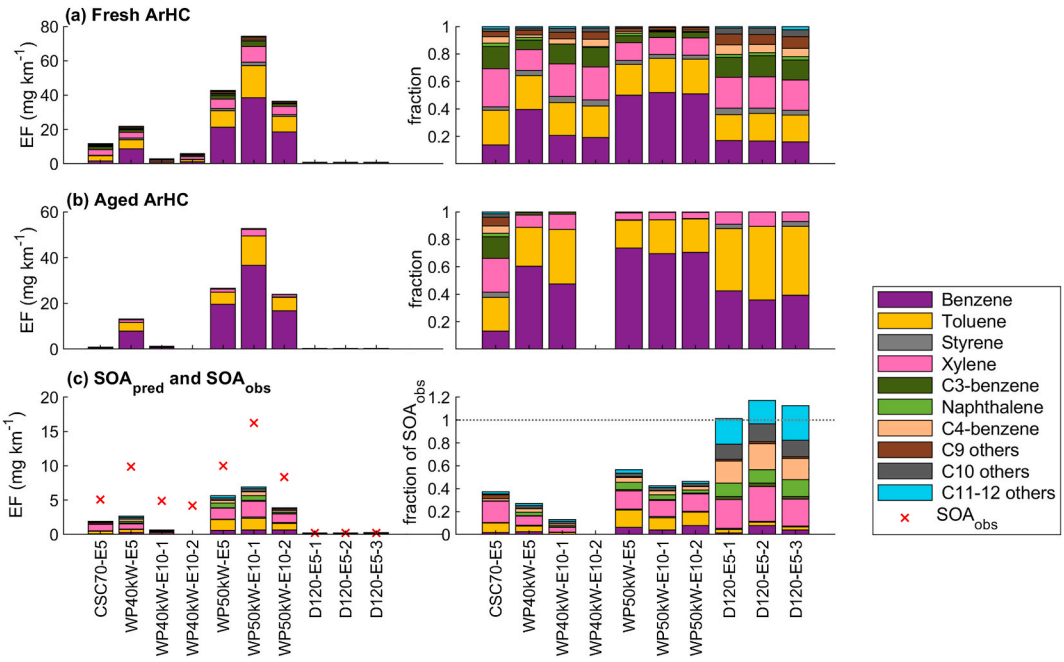

Fig. 2. ArHC emissions from a gasoline vehicle: the absolute ArHC emission factors and their relative share in the fresh (a) and aged exhaust at the end of each experiment (b), and the SOA predicted to have formed from the observed species compared to the observed SOA formation (SOA_{obs}) measured by the SP-AMS (c). (Secondary PTR-ToF-MS data are not available for WP40 kW-E10.). (For interpretation of the references to color in this figure legend, the reader is referred to the Web version of this article.)

than 23 nm (PN23, including volatile particles) measured by FMPS from the tailpipe ranged from 1.3 to 3.5 × 10^6 km^{-1}. An exception was the WP40 kW experiment with B7, where the DPF was regenerated ('WP40 kW-B7-regen.') during sampling, which led to a two orders of magnitude increase in PM mass emissions. For the diesel experiments, primary particulate concentrations in the chamber were below the detection limit for both SP-AMS and the aethalometer. Similarly, OGC concentrations in the fresh diesel exhaust emissions were low compared to the gasoline vehicle: primary THC emissions measured by FID were in the range of 0.8–3.1 mg km^{-1}, while ArHC were not detectable using the PTR-ToF-MS.

3.2. *Primary emissions from the gasoline vehicle*

The PN23 emission from the gasoline vehicle was two orders of magnitude higher than that for the DPF-equipped diesel vehicle. This large difference was influenced by the absence of GPF in the gasoline vehicle in use. Among the studied conditions, the lowest PN23 emission factor of the gasoline vehicle was observed for CSC70, with a higher PN23 for E5 (4.6 × 10^{12} km^{-1}) than RFG (2.6 × 10^{12} km^{-1}). CSC70, however, emitted the most particulate mass due to the largest particle size: GMD (±GSD) was 89 nm (±1.8) for E5 gasoline and 79–80 (±1.9) for RFG. D120, WP40 kW, and WP50kW, on the other hand, emitted PN23 concentrations in the range of 4.7 × 10^{12}–1.2 × 10^{13} km^{-1}. The particles emitted under these conditions were, however, relatively small, with GMD (±GSD) values of 46–50 nm (±1.7), 42–51 nm (±1.6–1.8), and 40–41 nm (±1.7–1.9), respectively. Consequently, the particulate mass emissions were lower than those in CSC70. Particulate mass emission factors measured by SP-AMS ranged from 0.6 to 2.9 mg km^{-1} (Fig. 1a, Table S2). In all engine conditions with all gasoline fuels, the majority (over 85%) of primary particulate mass measured by SP-AMS was rBC, while OA formed less than 10% of the particulate mass (except for WP40 kW operation with E10 gasoline) (Fig. 1a).

The optically derived eBC mass concentration was in good agreement with rBC for CSC70. For other conditions, the aethalometer-based eBC was typically at least a factor of 1.5 higher than the mass of submicron rBC determined by SP-AMS. Such a discrepancy may be due to the lowered collection efficiency of SP-AMS in the sub-50 nm size range as well as differences in the actual and default soot mass absorption coefficients. The AAEs of the primary gasoline aerosol ranged from 1.15 to 1.29 with no discernible dependence on experimental conditions.

Primary organic aerosol (POA) had in all cases O:C ratios of close to zero and H:C ratios of approximately 2, which indicates that gasoline POA is composed of hydrocarbon-like OA(Ng et al., 2011). Such low O:C ratios have also previously been measured for Euro5-level vehicles(Collier et al., 2015; Platt et al., 2013), while O:C ratios reported for GDI vehicles adhering to pre-Euro6 standards have been typically slightly higher (in the range of 0.1–0.4(Nordin et al., 2013; Presto et al., 2014; Timonen et al., 2017)). The observed elemental compositions support previous findings indicating that unburned motor oil can be an important contributor to POA emission from GDI vehicles(Drozd et al., 2019; Worton et al., 2014; Zhao et al., 2017).

THC emissions measured from the tailpipe by FID were the highest for high power operation (155–165 mg C km^{-1}), while D120

emitted the lowest THC amounts among all gasoline vehicle experiments (below 10 mg C km^{-1}). For CSC70, average THC emission was 16–19 mgC km^{-1}. However, it should be noted that for CSC70, the majority of the organic gases were emitted within the first few minutes of driving from cold start, when the TWC was not yet fully operational (Figure S8). In this period, the emission of both gaseous hydrocarbons and particulate matter were up to one order of magnitude higher than during the steady state operation, and, thus, contributed excessively to the emissions.

The organic gaseous emissions in the E5 and E10 experiments were further analyzed from the PTR-ToF-MS data collected from the chamber before the aging process was started. In total 82 ions were identified from the spectra with concentrations above detection limit in at least one experiment (Table S4). Most of the detected compounds can be considered volatile organic compounds (VOCs). The share of higher molecular weight intermediate-(I)VOCs (with saturation vapor pressure below 3×10^6 μg m^{-3}), namely, C11- and C12-aromatics, to the total ArHC was below 5% in all E5 experiments. The observed gaseous species were dominated by ArHC, as expected based on previous assessments of vehicular OGC emissions(Liu et al., 2015; Peng et al., 2017; Pieber et al., 2018). The rest of the quantified ions originated mainly from small carbonylic compounds, namely, m/z 45.03 (acetaldehyde) and m/z 59.05 (acetone/-propanal), and small hydrocarbons, namely, m/z 43.06 (propene) and m/z 57.07 (butene). It should, however, be noted that while PTR is a relatively soft ionization method, these small ion masses may also include fragmentation products from larger molecules. EFs of all the observed OGCs are presented in Figure S9. Further, it is important to note that, for example, the long-chained alkanes that are likely present in the exhaust emissions have too low protonation affinity to be detected by the PTR-ToF-MS.

The main aromatic compounds were similar in all experiments, namely, benzene, toluene, and xylene/ethylbenzene, although their emission factors depended highly on the fuel and engine conditions. Fig. 2a reports the ArHC EFs for the gasoline vehicle as measured in fresh exhaust per kilometer as well as their relative percentage over the total measured ArHC amount. For E5, the highest ArHC emission was produced by high engine load operation (22 mg km^{-1} for WP40 kW, 42 mg km^{-1} for WP50kW), while CSC70 emitted 12 mg km^{-1} and D120 emitted only 0.8–0.9 mg km^{-1}. For high-power operation with E10, the emission factors were 3–6 mg km^{-1} for WP40 kW and 36–74 mg km^{-1} for WP50kW. The shares of the observed compounds relative to total ArHC concentrations are consistent with those previously measured for the exhaust emissions of Euro4-5 vehicles(Bahreini et al., 2012; Liu et al., 2015; Pieber et al., 2018). High engine load operation, however, led to relatively higher shares of benzene compared to other operation modes. Namely, benzene accounted for 40% or 50% of total ArHC EF for WP40 kW and WP50kW, respectively, compared to 14–17% in the other conditions. This affects also the emitted toluene-to-benzene ratios, which are sometimes used for source apportionment in urban air studies(Bahreini et al., 2012; Borbon et al., 2018; Halliday et al., 2016; Kerimray et al., 2020). The toluene-to-benzene ratios in the fresh exhaust for WP40 kW, WP50kW, CSC70, and D120 with E5 gasoline were 0.6, 0.5, 1.8, and 1.2, respectively. The respective ratios for E10 gasoline were 1.2 for WP40 kW and 0.5 for WP50kW. Overall, the observed ratios are relatively low compared to prior assessments, which have resulted in a toluene-to-benzene ratios greater than 2 for fresh traffic emissions(Bahreini et al., 2012; Heeb et al., 2000; Kumar et al., 2020; Liu et al., 2015). Thus, the low toluene-benzene ratios of new generation vehicle emissions should be considered when using these ratios for the indication of emission sources or photochemical processing in ambient air.

3.3. Secondary particulate matter formation from diesel exhaust emissions

Only negligible secondary aerosol emissions were measured for the diesel vehicle, as expected based on the low THC emissions. Secondary emission factors could be determined for CSC70 and for the DPF regeneration phase (Fig. 1b). For the other diesel experiments, the low CS_{PM} was similar as in the blank experiments due to the practically non-existent primary particle emissions (Figure S2). This restrains the secondary particle formation, as consequently a major share of the LVOCs emitted or formed would remain in the gas phase (Figure S4). However, even in the diesel experiments, at least one fifth of the LVOCs were estimated to condense onto the particles. Because formation of SOA could not be observed, the LVOC concentrations must have been correspondingly low (below roughly 50 μg km^{-1}, assuming that only one fifth of the LVOC condenses to particulate phase). In addition, the low EFs of directly emitted secondary aerosol precursors confirm previous assessments of negligible secondary aerosol production from DPF-equipped diesel passenger vehicles(Chirico et al., 2010; Platt et al., 2017; Zhao et al., 2017). On the other hand, new generation Euro6-level diesel vehicles can notably influence atmospheric processes by, for example, altering the availability of NO_x in ambient air, which also impacts the SOA yields from aromatic precursors from other sources. As a consequence, the general reduction in NO_x emissions upon vehicle fleet renewal can lead to enhancements in the urban SOA production potential of precursors from other sources (Gentner et al., 2017). NO_x emissions emitted by the diesel vehicle (2–430 mg NO km^{-1} in primary exhaust), however, remain significant also with respect to the SIA formation potential of ambient air despite the strong reduction achieved via the SCR system (Kostenidou et al., 2021).

3.4. Secondary particulate matter formation from gasoline exhaust emissions

Total particulate mass EFs in E5 exhaust increased during the 24-h atmospheric equivalent photochemical exposure up to 1.1–1.5 mg km^{-1}, 30 mg km^{-1}, 122 mg km^{-1}, and 119 mg km^{-1} for D120, CSC70, WP40 kW, and WP50kW, respectively, underlining the importance of high engine load conditions on secondary particulate matter potential of the vehicular emissions (Fig. 1b). Maximum PM enhancement ratios (ERs, indicating the ratio between the total EFs after aging and primary aerosols) during the full photochemical aging process were determined to be 1.9, 12, 470, and 130 for D120, CSC70, WP40 kW, and WP50kW, respectively. The large range for the ERs complies with previously observed secondary formation in Euro5-level gasoline vehicles with different engine operation conditions. In previous OFR studies of transient cycles, enhanced ERs have been noted for cold start periods and acceleration events (Karjalainen et al., 2016; Kuittinen, McCaffery, Peng, et al., 2021; Link et al., 2017; Pieber et al., 2018; Timonen et al., 2017).

Previously, modern gasoline passenger vehicles operated on standard testing cycles have been noted to induce ERs of roughly 1.5–15, when averaged over the test cycles. Thus, the ER induced by the high engine power operation is drastically higher compared to transient cycles, whereas the secondary aerosol potential in D120 is in the lower range compared to previous findings (Gramsch et al., 2018; Karjalainen et al., 2016; Timonen et al., 2017).

High quantities of secondary particulate NH_4NO_3 were formed during photochemical aging of gasoline exhaust when the vehicle was operated under high engine power and for CSC70 (Fig. 1b). The molar ratios of NO_3 and NH_4 measured by the SP-AMS were identical (Figure S6), indicating that secondary NO_3 was purely in inorganic form. The maximum SIA formation in terms of emission factors was determined to be 277, 211, 25, and 0.4 mg km^{-1} for WP40 kW, WP50kW, CSC70, and D120, respectively. For RFG, no SIA was observed in WP40 kW or D120. This can be explained by the low NH_3 emissions from RFG in these driving conditions, since NH_3 concentration was limiting the NH_4NO_3 formation in the chamber. In CSC70, however, both the NH_3 emission and SIA formation potential of RFG exhaust (maximum of 25 mg km^{-1}) was similar to the gasoline fuels with lower alcohol content. NH_3 is formed as a byproduct in gasoline vehicle three-way catalysts, particularly under high power operation (Table S2). Given the relative humidity (55 $\pm$ 5%) and temperature (23 $\pm$ 2 °C) prevailing in the chamber, NH_4NO_3 is expected to exist as solid particles. The generated NH_3 was converted to particulate NH_4NO_3 by the reaction with HNO_3, which is formed from NO_x during photochemical processing. It should be noted that the vapor pressure of NH_4NO_3 is very temperature dependent, and based on the Clausius-Clapeyron relationship the maximum 2 °C increase in temperature during an experiment was sufficient to increase the vapor pressure by over 50%, causing considerable evaporation especially in the RFG CSC70 experiments. Substantial formation of NH_4NO_3 in urban traffic exhaust has been previously noted by, e.g., Tkacik et al. (2014) and Link et al. (2017). Our results indicate that TWC-equipped vehicles can give rise to locally high concentrations of NH_4NO_3 and that they may upon further dilution or oxidation of gaseous components also act as a source for NH_3 and HNO_3 pollutants when transported in the atmosphere.

The SOA formation potential of gasoline exhaust was highly dependent on engine operation: the SOA emission factors of E5 gasoline exhaust were determined to be 10, 10, 5.1, and 0.19–0.24 mg km^{-1} for WP40 kW, WP50kW, CSC70, and D120, respectively. For reformulated gasoline, SOA EFs for WP40 kW and CSC70 were determined to be 0.7 and 6.1 mg km^{-1}, respectively. The observed SOA potentials are comparable with previously reported averaged SOA EFs from dynamic test cycles, with D120 being in the lower and high engine power conditions in the upper range of the EFs reported for modern gasoline vehicles (Gordon et al., 2014; Kuittinen, McCaffery, Peng, et al., 2021; Park et al., 2021; Peng et al., 2017; Pieber et al., 2018). The results highlight that prolonged high engine load and cold start conditions can have a major importance on secondary organic aerosol generation of EURO6 gasoline cars. Under the WP40 kW condition, the SOA EFs for E10 and RFG were lower than those measured for E5 gasoline, which might be influenced by the higher alcohol contents in E10 and RFG fuels, as suggested by earlier studies (Gramsch et al., 2018; Kuittinen, McCaffery, Zimmerman, et al., 2021; Timonen et al., 2017). However, in other conditions, the SOA EFs and the OA ERs (Fig. 1c) were similar for the RFG as for traditional E5 and E10. Overall, no systematic effect of fuel reformulation could be observed in the secondary aerosol formation potential. It should be noted that, in addition to the use of variable fuel reformulations, real-life driving also involves transient engine conditions, whose effects on secondary aerosol formation are not assessed in this work, whereas this study includes a number of different driving conditions under constant velocity and wheel load. Nevertheless, the selected driving conditions provide a large variation in exhaust gas compositions to correlate the secondary aerosol formation potential with their precursor gases. Further, the high engine load conditions are shown to induce high secondary aerosol potential, regardless of the fuel reformulation.

The rBC concentrations determined by SP-AMS increased slightly during aging. This is likely partly due to the growth of initially sub-50nm sized particles to a more efficiently measured size range and partly due to the increased coating and compaction of the initially agglomerated soot, which is linked with the enhanced collection efficiency of SP-AMS(Willis et al., 2014). Similar phenomena

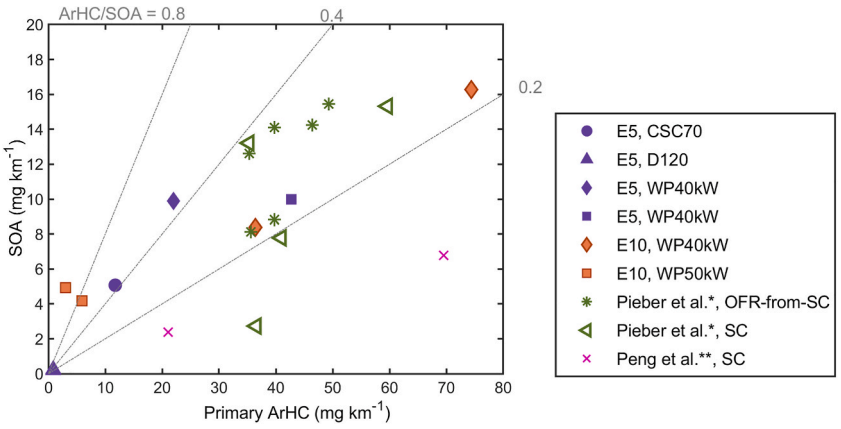

Fig. 3. Correlation of the primary ArHC EF to SOA EFs at the end of each experiment, with the straight lines displaying ArHC/SOA ratios of 0.2, 0.4, and 0.8. Additional data from (*) Euro5-6 -level GDI vehicles with SOA sampled either from a smog chamber (SC) or downstream of an oxidation flow reactor connected to the SC (OFR-from-SC) by Pieber et al. (2018) and (**) port gasoline injection (PFI) vehicle (China IV) after TWC, measured using a SC, by Peng et al. (2017). (For interpretation of the references to color in this figure legend, the reader is referred to the Web version of this article.)

have also been noted by others when aging gasoline exhaust with high SOA formation potential (Timonen et al., 2017).

Majority of secondary aerosol mass formation took place during the first 24 eqv.h. The temporal evolution of PM mass and chemical compositions during photochemical aging is presented for each combination of fuel and driving condition in the Supplementary Information, Figure S10. New particle formation via nucleation of the reactive gases was observed especially in the WP50kW and CSC70 exhaust, where a second size mode was formed within the first hour of photochemical exposure (Figure S5). New particle formation via nucleation was evident in the smallest observed size ranges (sub-10 nm). Nucleation was also observed in the diesel and blank experiments, where the primary particulate concentrations in the chamber were very low. For D120 exhaust, no new modes were detected during aging. Instead, in this condition, the particle growth was driven by condensation of vapors on the existing particles, whose GMD increased by a factor of 1.5 ± 0.09.

3.5. *Transformation of organic gaseous emissions*

Fig. 2a and b shows the ArHC emission factors (mg km^{-1}) measured in the fresh and photochemically aged exhaust for the E5 and E10 gasoline vehicle experiments. The photochemical decay of the ArHC observed by PTR-ToF-MS was generally in line with their reported OH reactivities. The slowest decay in ArHC was observed for the high-power operating conditions due to the high relative benzene content in the primary exhaust. There, the total ArHC decay was in the range of 30–40%. Under other conditions, the more reactive xylene and C3-benzenes formed a higher portion of the ArHC emission factor, subsequently leading to higher total ArHC decay (63–94%).

The formation of SOA was strongly related to the ArHC content in the fresh exhaust, as shown in Fig. 3. This analysis also includes previously published EFs for Euro5-6 -level gasoline vehicles(Peng et al., 2017; Pieber et al., 2018). The ratio of SOA formation to the decay in observed aromatic SOA precursors (ΔOA/ΔArHC) was 0.32 ± 0.02 for highway driving, 0.65 for CSC70, and 1.1 for WP40 kW. These ratios resemble the ΔOA/ΔArHC previously observed for new generation passenger cars operated with different running cycles, with the exception of the measurements of idling gasoline vehicle exhausts for which lower ratios have been measured(Liu et al., 2015; Nordin et al., 2013; Pieber et al., 2018; Zhao et al., 2018).

In general, the effective SOA yields of ArHC depend especially on the composition of OGC emission, but are also influenced by the overall exhaust composition, such as OGC/NO_x ratio. A bottom-up estimation of SOA formation in E5 and E10 exhaust was performed based on the decay of aromatic compounds and by applying literature SOA yields (in the range of 0.1–0.7 in 'low-NO_x' conditions; see Table S4). On this basis, the majority of SOA formation predicted based on ArHC decay (SOA_{pred}) was estimated to be derived from the reaction products of xylene and toluene (Fig. 2c). For D120, the ratio SOA_{pred} to SOA observed by SP-AMS (SOA_{obs}) was 1.1–1.2; in other words, all SOA formation from D120 can be explained by the observed decay of traditional aromatic precursors. For other driving cycles, the fraction of unexplained SOA_{obs} is higher, with SOA_{pred}-to-SOA_{obs} ratios of 0.47, 0.27, and 0.6 for CSC70, WP40 kW, and WP50kW with E5 gasoline, respectively. This indicates that in high power engine conditions and in the cold start conditions, IVOCs released from unburned lubrication oil may have played an important role in the SOA budget, as observed previously by Zhao et al. (2017). These compounds include, for example, long chain aliphatic compounds, which have relatively low SOA yields compared to aromatic precursors(Gordon et al., 2014). They can, however, contribute to SOA formation notably if their primary concentrations are high. Furthermore, aromatic IVOCs likely present in the exhaust have significantly higher SOA yields than the lighter aromatics observed by PTR-ToF-MS(Gordon et al., 2014; Zhao et al., 2016).

The exact oxidation and functionalization pathways, and, consequently, the resulting secondary aerosol formation potential of an exhaust depend on the prevailing chemistry, such as the availability of the various oxidants, the OGC/NO_x ratio, and the available

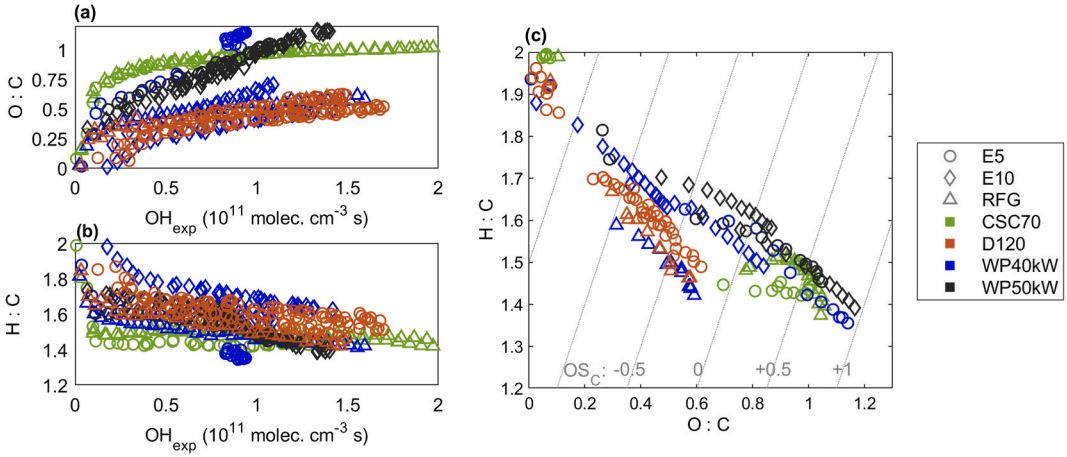

Fig. 4. Development of the OA elemental composition during photochemical aging as the function of the OH exposure (a–b) and in the Van Krevelen space (c) in exhausts of the different gasoline fuels (indicated by marker type) and engine operation conditions (indicated by marker color). (For interpretation of the references to color in this figure legend, the reader is referred to the Web version of this article.)

surface area of particles that serve as condensation seeds for SOA formation. The conditions in the chamber can be generally considered 'low-NO_x' (except for the primary conditions in the cold start experiments; see Figure S11), which dictates the SOA yields by altering the pathways for the peroxy radical reactions following the initial OH oxidation. When NO availability is limited, the SOA yields for ArHC are typically higher than the case when high quantities of NO are available for the oxidation of the reaction products (Hildebrandt et al., 2009; Ng et al., 2007). NO_x saturated conditions have traditionally been considered to prevail in polluted ambient air close to traffic. In future, technical improvements, such as the use of SCR for diesel vehicles and electrification of transport fleet, will efficiently decrease the concentrations of NO_x, which needs to be considered when estimating the SOA formation potential for urban emission sources.

3.6. Effect of photochemical aging on particulate matter composition

Whereas SOA formation occurred mainly during the first hour, $\overline{OS}_C$ continued to increase with an Δ H:C/Δ O:C -ratio of (−1.0) – (−0.50) during the aging experiments (Fig. 4c). Most of the increase happened within the first 24 eqv.h alongside the majority of SOA formation, due to SOA being more oxidized than organic carbon in the primary aerosol. The continuous increase in $\overline{OS}_C$ was then likely caused by heterogeneous oxidation of OA. The observed changes agree well with those observed previously for aromatic precursors (Δ H:C/Δ O:C -ratios −0.87 to −0.45)(Lambe et al., 2011) and with ambient observations of OA transformation under photochemical conditions(Ng et al., 2011).

The IR absorption of gasoline exhausts strongly increased during the aging experiments, roughly simultaneously with secondary aerosol formation (Fig. 5). The increase in IR absorption was the most dominant in the conditions with highest secondary aerosol formation, namely, under CSC70 and WP50kW conditions and WP40 kW with E5 fuel. The IR attenuation was below the aethalometer detection limit for the diesel-engine experiments.

For E5 gasoline, the light absorption for WP40 kW and WP50kW exhaust particles increased relatively more in the infrared region than at lower wavelengths, resulting in an AAE of 0.6 and 1.1 at 24 eqv.h, respectively (Figure S12). For CSC70, on the other hand, the secondary AAE was 0.8 at the minimum but rose to 1.4 upon further aging. For D120, AAE and IR absorption remained stable as a result of minor formation of secondary coating. The results agree with previously observed low AAEs in engine exhausts containing bimodal particle size distributions (Helin et al., 2021).

Changes in IR absorption and AAE during photochemical aging of vehicular exhaust are expected, as the wavelength-dependent light absorption can be considered to be governed by two aspects: i) optical lensing and ii) chemical changes. Assuming that the secondary aerosol forms a spherical shell around the primary particle cores, the increase in the shell volume fraction impacts the aerosol optical properties in accordance with Mie theory (Virkkula, 2021). The increase in AAE may also be due to the formation of organic brown carbon, which absorbs light particularly at shorter wavelengths.

4. Conclusions

This study shows that secondary aerosols dominate the contribution of Euro6-level gasoline passenger vehicles to ambient air particulate matter, agreeing with several previous secondary aerosol potential studies on modern gasoline car exhaust emissions (e.g. Gordon et al., 2014; Pieber et al., 2018; Kuittinen, McCaffery, Peng, et al., 2021; Kuittinen et al., 2021; Timonen et al., 2017). Our experiments indicate that cold start and prolonged high engine loads, such as uphill driving or high speed driving at highways, can substantially increase both secondary organic aerosol and secondary inorganic aerosol formation potentials of gasoline passenger vehicles. These conditions are typically not fully covered when studying the aging of exhaust from the standard driving cycles, and special focus should be paid on those when assessing the impact of modern gasoline fleet on ambient air.

The relatively high SOA potential of the modern gasoline vehicle exhausts was largely related to the primary ArHC emissions. In addition, substantial formation of secondary NH_4NO_3 can occur when high quantities of (currently unregulated) NH_3 are emitted, as shown here especially for high engine load operation. On the other hand, new diesel vehicles can be expected to lead to negligible SOA formation due to the low organic primary emissions in the gas phase. Instead, the most notable air quality impact of diesel exhaust lies in the substantial NO_x emissions.

While there were large differences observed between gasoline and diesel exhaust, no systematic effects of gasoline fuel reformulations on the secondary aerosol formation potentials were observed. The similarity of exhaust emissions and their secondary aerosol formation potential between the different gasoline fuels with different alcohol contents may be due to similarities in the contents of fuel aromatics, which are the major precursors for SOA. The results obtained from the reformulated fuels confirm that tailpipe gaseous aromatic emissions are a reasonable proxy for estimating the SOA formation potential of Euro6 gasoline exhaust, although they did not cover the full SOA potential in the cold start and high engine load conditions. Thus, SOA formation of gasoline vehicles could be indirectly controlled by regulation of the gaseous aromatic species. Overall, future legislation aimed at automotive emissions should focus on limiting the secondary aerosol formation potential of vehicular emissions, including both exhaust SOA precursors and NH_3.

Finally, it remains critical to consider that the formation of secondary aerosols affects the optical properties of the exhaust emissions, as observed in this study. This should be further studied to assess the climate effects of vehicular exhaust aerosols.

Declaration of competing interest

The authors declare that they have no known competing financial interests or personal relationships that could have appeared to

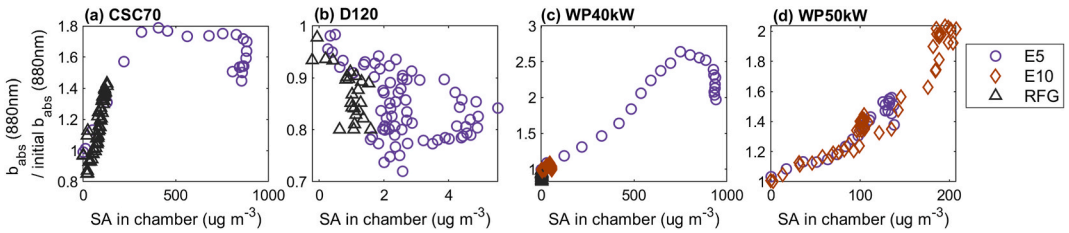

Fig. 5. Evolution of infrared light absorption (at 880 nm) of exhaust particles as the function of secondary aerosol mass concentration with different gasoline fuels and driving conditions. (For interpretation of the references to color in this figure legend, the reader is referred to the Web version of this article.)

influence the work reported in this paper.

Data availability

Data will be made available on request.

Acknowledgments

The experimental work was financially supported by the Horizon 2020 research and innovation program through the EURO-CHAMP-2020 Infrastructure Activity (grant no. 730997). SMP acknowledges support from the Swiss National Science Foundation under project number P400P2_194390. We thank Norbert Heeb (Empa) and Pierre Comte (Bern University of Applied Sciences) for providing the additional fuel use data from the CCEM project GasOMeP that were used to convert the emission factors from Pieber et al. (2018, https://doi.org/10.5194/acp-18-9929-2018) and Pieber et Prevot (2018, https://doi.org/10.5281/zenodo.1305770) to a "per km" basis.

Appendix A. Supplementary data

Supplementary data related to this article can be found at https://doi.org/10.1016/j.jaerosci.2023.106159.

References

Bahreini, R., Middlebrook, A. M., de Gouw, J. A., Warneke, C., Trainer, M., Brock, C. A., Stark, H., Brown, S. S., Dube, W. P., Gilman, J. B., Hall, K., Holloway, J. S., Kuster, W. C., Perring, A. E., Prevot, A. S. H., Schwarz, J. P., Spackman, J. R., Szidat, S., Wagner, N. L., … Parrish, D. D. (2012). Gasoline emissions dominate over diesel in formation of secondary organic aerosol mass. *Geophysical Research Letters, 39*(6). https://doi.org/10.1029/2011GL050718. n/a-n/a.

Barmet, P., Dommen, J., DeCarlo, P. F., Tritscher, T., Praplan, A. P., Platt, S. M., Prévôt, A. S. H., Donahue, N. M., & Baltensperger, U. (2012). OH clock determination by proton transfer reaction mass spectrometry at an environmental chamber. *Atmospheric Measurement Techniques, 5*(3), 647–656. https://doi.org/10.5194/amt-5-647-2012

Borbon, A., Boynard, A., Salameh, T., Baudic, A., Gros, V., Gauduin, J., Perrussel, O., & Pallares, C. (2018). Is traffic still an important emitter of monoaromatic organic compounds in European urban areas? *Environmental Science and Technology, 52*(2), 513–521. https://doi.org/10.1021/acs.est.7b01408

Canagaratna, M. R., Onasch, T. B., Wood, E. C., Herndon, S. C., Jayne, J. T., Cross, E. S., Miake-Lye, R. C., Kolb, C. E., & Worsnop, D. R. (2010). Evolution of vehicle exhaust particles in the atmosphere. *Journal of the Air & Waste Management Association, 60*(10), 1192–1203. https://doi.org/10.3155/1047-3289.60.10.1192

Chirico, R., DeCarlo, P. F., Heringa, M. F., Tritscher, T., Richter, R., Prévôt, A. S. H., Dommen, J., Weingartner, E., Wehrle, G., Gysel, M., Laborde, M., & Baltensperger, U. (2010). Impact of aftertreatment devices on primary emissions and secondary organic aerosol formation potential from in-use diesel vehicles: Results from smog chamber experiments. *Atmospheric Chemistry and Physics, 10*(23), 11545–11563. https://doi.org/10.5194/acp-10-11545-2010

Collier, S., Zhou, S., Kuwayama, T., Forestieri, S., Brady, J., Zhang, M., Kleeman, M., Cappa, C., Bertram, T., & Zhang, Q. (2015). Organic PM emissions from vehicles: Composition, O/C ratio, and dependence on PM concentration. *Aerosol Science and Technology, 49*(2), 86–97. https://doi.org/10.1080/02786826.2014.1003364

Drozd, G. T., Zhao, Y., Saliba, G., Frodin, B., Maddox, C., Oliver Chang, M.-C., Maldonado, H., Sardar, S., Weber, R. J., Robinson, A. L., & Goldstein, A. H. (2019). Detailed speciation of intermediate volatility and semivolatile organic compound emissions from gasoline vehicles: Effects of cold-starts and implications for secondary organic aerosol formation. *Environmental Science and Technology, 53*(3), 1706–1714. https://doi.org/10.1021/acs.est.8b05600

Gentner, D. R., Jathar, S. H., Gordon, T. D., Bahreini, R., Day, D. A., El Haddad, I., Hayes, P. L., Pieber, S. M., Platt, S. M., de Gouw, J., Goldstein, A. H., Harley, R. A., Jimenez, J. L., Prévôt, A. S. H., & Robinson, A. L. (2017). Review of urban secondary organic aerosol formation from gasoline and diesel motor vehicle emissions. *Environmental Science and Technology, 51*(3), 1074–1093. https://doi.org/10.1021/acs.est.6b04509

Gordon, T. D., Presto, A. A., May, A. A., Nguyen, N. T., Lipsky, E. M., Donahue, N. M., Gutierrez, A., Zhang, M., Maddox, C., Rieger, P., Chattopadhyay, S., Maldonado, H., Maricq, M. M., & Robinson, A. L. (2014). Secondary organic aerosol formation exceeds primary particulate matter emissions for light-duty gasoline vehicles. *Atmospheric Chemistry and Physics, 14*(9), 4661–4678. https://doi.org/10.5194/acp-14-4661-2014

Gramsch, E., Papapostolou, V., Reyes, F., Vásquez, Y., Castillo, M., Oyola, P., López, G., Cádiz, A., Ferguson, S., Wolfson, M., Lawrence, J., & Koutrakis, P. (2018). Variability in the primary emissions and secondary gas and particle formation from vehicles using bioethanol mixtures. *Journal of the Air & Waste Management Association, 68*(4), 329–346. https://doi.org/10.1080/10962247.2017.1386600

Guan, B., Zhan, R., Lin, H., & Huang, Z. (2014). Review of state of the art technologies of selective catalytic reduction of NOx from diesel engine exhaust. *Applied Thermal Engineering, 66*(1–2), 395–414. https://doi.org/10.1016/j.applthermaleng.2014.02.021

Halliday, H. S., Thompson, A. M., Wisthaler, A., Blake, D. R., Hornbrook, R. S., Mikoviny, T., Müller, M., Eichler, P., Apel, E. C., & Hills, A. J. (2016). Atmospheric benzene observations from oil and gas production in the Denver-Julesburg Basin in July and August 2014. *Journal of Geophysical Research: Atmospheres, 121*(18). https://doi.org/10.1002/2016JD025327, 11,055-11,074.

Hao, L. Q., Romakkaniemi, S., Yli-Pirilä, P., Joutsensaari, J., Kortelainen, A., Kroll, J. H., Miettinen, P., Vaattovaara, P., Tiitta, P., Jaatinen, A., Kajos, M. K., Holopainen, J. K., Heijari, J., Rinne, J., Kulmala, M., Worsnop, D. R., Smith, J. N., & Laaksonen, A. (2011). Mass yields of secondary organic aerosols from the oxidation of α-pinene and real plant emissions. *Atmospheric Chemistry and Physics, 11*(4), 1367–1378. https://doi.org/10.5194/acp-11-1367-2011

Heald, C. L., & Kroll, J. H. (2020). The fuel of atmospheric chemistry: Toward a complete description of reactive organic carbon. *Science Advances, 6*(6). https://doi.org/10.1126/sciadv.aay8967

Heeb, N. V., Forss, A.-M., Bach, C., Reimann, S., Herzog, A., & Jäckle, H. W. (2000). A comparison of benzene, toluene and C2-benzenes mixing ratios in automotive exhaust and in the suburban atmosphere during the introduction of catalytic converter technology to the Swiss Car Fleet. *Atmospheric Environment, 34*(19), 3103–3116. https://doi.org/10.1016/S1352-2310(99)00446-X

Helin, A., Virkkula, A., Backman, J., Pirjola, L., Sippula, O., Aakko-Saksa, P., Väätäinen, S., Mylläri, F., Järvinen, A., Bloss, M., Aurela, M., Jakobi, G., Karjalainen, P., Zimmermann, R., Jokiniemi, J., Saarikoski, S., Tissari, J., Rönkkö, T., Niemi, J., & Timonen, H. (2021). Variation of absorption angstrom exponent in aerosols from different emission sources. *Journal of Geophysical Research: Atmospheres, 126*, Article e2020JD034094. https://doi.org/10.1029/2020JD034094

Hildebrandt, L., Donahue, N. M., & Pandis, S. N. (2009). High formation of secondary organic aerosol from the photo-oxidation of toluene. *Atmospheric Chemistry and Physics, 9*(9), 2973–2986. https://doi.org/10.5194/acp-9-2973-2009

Hooftman, N., Messagie, M., Van Mierlo, J., & Coosemans, T. (2018). A review of the European passenger car regulations – real driving emissions vs local air quality. *Renewable and Sustainable Energy Reviews, 86*, 1–21. https://doi.org/10.1016/j.rser.2018.01.012

Jordan, A., Haidacher, S., Hanel, G., Hartungen, E., Märk, L., Seehauser, H., Schottkowsky, R., Sulzer, P., & Märk, T. D. (2009). A high resolution and high sensitivity proton-transfer-reaction time-of-flight mass spectrometer (PTR-TOF-MS). *International Journal of Mass Spectrometry, 286*(2–3), 122–128. https://doi.org/10.1016/j.ijms.2009.07.005

Karjalainen, P., Timonen, H., Saukko, E., Kuuluvainen, H., Saarikoski, S., Aakko-Saksa, P., Murtonen, T., Bloss, M., Dal Maso, M., Simonen, P., Ahlberg, E., Svenningsson, B., Brune, W. H., Hillamo, R., Keskinen, J., & Rönkkö, T. (2016). Time-resolved characterization of primary particle emissions and secondary particle formation from a modern gasoline passenger car. *Atmospheric Chemistry and Physics, 16*(13), 8559–8570. https://doi.org/10.5194/acp-16-8559-2016

Kerimray, A., Baimatova, N., Ibragimova, O. P., Bukenov, B., Kenessov, B., Plotitsyn, P., & Karaca, F. (2020). Assessing air quality changes in large cities during COVID-19 lockdowns: The impacts of traffic-free urban conditions in Almaty, Kazakhstan. *The Science of the Total Environment, 730*, Article 139179. https://doi.org/10.1016/j.scitotenv.2020.139179

Kostenidou, E., Martinez-Valiente, A., R'Mili, B., Marques, B., Temime-Roussel, B., Durand, A., André, M., Liu, Y., Louis, C., Vansevenant, B., Ferry, D., Laffon, C., Parent, P., & D'Anna, B. (2021). Technical note: Emission factors, chemical composition, and morphology of particles emitted from Euro 5 diesel and gasoline light-duty vehicles during transient cycles. *Atmospheric Chemistry and Physics, 21*(6), 4779–4796. https://doi.org/10.5194/acp-21-4779-2021

Kuittinen, N., McCaffery, C., Peng, W., Zimmerman, S., Roth, P., Simonen, P., Karjalainen, P., Keskinen, J., Cocker, D. R., Durbin, T. D., Rönkkö, T., Bahreini, R., & Karavalakis, G. (2021). Effects of driving conditions on secondary aerosol formation from a GDI vehicle using an oxidation flow reactor. *Environmental Pollution, 282*, Article 117069. https://doi.org/10.1016/j.envpol.2021.117069

Kuittinen, N., McCaffery, C., Zimmerman, S., Bahreini, R., Simonen, P., Karjalainen, P., Keskinen, J., Rönkkö, T., & Karavalakis, G. (2021). Using an oxidation flow reactor to understand the effects of gasoline aromatics and ethanol levels on secondary aerosol formation. *Environmental Research, 200*, Article 111453. https://doi.org/10.1016/j.envres.2021.111453

Kumar, A., Sinha, V., Shabin, M., Hakkim, H., Bonsang, B., & Gros, V. (2020). Non-methane hydrocarbon (NMHC) fingerprints of major urban and agricultural emission sources for use in source apportionment studies. *Atmospheric Chemistry and Physics, 20*(20), 12133–12152. https://doi.org/10.5194/acp-20-12133-2020

Lambe, A. T., Onasch, T. B., Massoli, P., Croasdale, D. R., Wright, J. P., Ahern, A. T., Williams, L. R., Worsnop, D. R., Brune, W. H., & Davidovits, P. (2011). Laboratory studies of the chemical composition and cloud condensation nuclei (CCN) activity of secondary organic aerosol (SOA) and oxidized primary organic aerosol (OPOA). *Atmospheric Chemistry and Physics, 11*(17), 8913–8928. https://doi.org/10.5194/acp-11-8913-2011

Leskinen, A., Yli-Pirilä, P., Kuuspalo, K., Sippula, O., Jalava, P., Hirvonen, M.-R., Jokiniemi, J., Virtanen, A., Komppula, M., & Lehtinen, K. E. J. (2015). Characterization and testing of a new environmental chamber. *Atmospheric Measurement Techniques, 8*(6), 2267–2278. https://doi.org/10.5194/amt-8-2267-2015

Link, M. F., Kim, J., Park, G., Lee, T., Park, T., Babar, Z. B., Sung, K., Kim, P., Kang, S., Kim, J. S., Choi, Y., Son, J., Lim, H.-J., & Farmer, D. K. (2017). Elevated production of NH4NO3 from the photochemical processing of vehicle exhaust: Implications for air quality in the Seoul Metropolitan Region. *Atmospheric Environment, 156*, 95–101. https://doi.org/10.1016/j.atmosenv.2017.02.031

Liu, T., Wang, X., Deng, W., Hu, Q., Ding, X., Zhang, Y., He, Q., Zhang, Z., Lü, S., Bi, X., Chen, J., & Yu, J. (2015). Secondary organic aerosol formation from photochemical aging of light-duty gasoline vehicle exhausts in a smog chamber. *Atmospheric Chemistry and Physics, 15*(15), 9049–9062. https://doi.org/10.5194/acp-15-9049-2015

Mejía-Centeno, I., Martínez-Hernández, A., & Fuentes, G. A. (2007). Effect of low-sulfur fuels upon NH3 and N2O emission during operation of commercial three-way catalytic converters. *Topics in Catalysis, 42*(1–4), 381–385. https://doi.org/10.1007/s11244-007-0210-2. *–43*.

Ng, N. L., Canagaratna, M. R., Jimenez, J. L., Chhabra, P. S., Seinfeld, J. H., & Worsnop, D. R. (2011). Changes in organic aerosol composition with aging inferred from aerosol mass spectra. *Atmospheric Chemistry and Physics, 11*(13), 6465–6474. https://doi.org/10.5194/acp-11-6465-2011

Ng, N. L., Kroll, J. H., Chan, A. W. H., Chhabra, P. S., Flagan, R. C., & Seinfeld, J. H. (2007). Secondary organic aerosol formation from m-xylene, toluene, and benzene. *Atmospheric Chemistry and Physics, 7*(14), 3909–3922. https://doi.org/10.5194/acp-7-3909-2007

Nordin, E. Z., Eriksson, A. C., Roldin, P., Nilsson, P. T., Carlsson, J. E., Kajos, M. K., Hellén, H., Wittbom, C., Rissler, J., Löndahl, J., Swietlicki, E., Svenningsson, B., Bohgard, M., Kulmala, M., Hallquist, M., & Pagels, J. H. (2013). Secondary organic aerosol formation from idling gasoline passenger vehicle emissions investigated in a smog chamber. *Atmospheric Chemistry and Physics, 13*(12), 6101–6116. https://doi.org/10.5194/acp-13-6101-2013

Palm, B. B., Campuzano-Jost, P., Ortega, A. M., Day, D. A., Kaser, L., Jud, W., Karl, T., Hansel, A., Hunter, J. F., Cross, E. S., Kroll, J. H., Peng, Z., Brune, W. H., & Jimenez, J. L. (2016). In situ secondary organic aerosol formation from ambient pine forest air using an oxidation flow reactor. *Atmospheric Chemistry and Physics, 16*(5), 2943–2970. https://doi.org/10.5194/acp-16-2943-2016

Park, G., Kim, K., Park, T., Kang, S., Ban, J., Choi, S., Yu, D.-G., Lee, S., Lim, S., Mun, S., Woo, J.-H., Jeon, C.-S., & Lee, T. (2021). Primary and secondary aerosols in small passenger vehicle emissions: Evaluation of engine technology, driving conditions, and regulatory standards. *Environmental Pollution, 286*, Article 117195. https://doi.org/10.1016/j.envpol.2021.117195

Peng, J., Hu, M., Du, Z., Wang, Y., Zheng, J., Zhang, W., Yang, Y., Qin, Y., Zheng, R., Xiao, Y., Wu, Y., Lu, S., Wu, Z., Guo, S., Mao, H., & Shuai, S. (2017). Gasoline aromatics: A critical determinant of urban secondary organic aerosol formation. *Atmospheric Chemistry and Physics, 17*(17), 10743–10752. https://doi.org/10.5194/acp-17-10743-2017

Pieber, S. M., Kumar, N. K., Klein, F., Comte, P., Bhattu, D., Dommen, J., Bruns, E. A., Kılıç, D., El Haddad, I., Keller, A., Czerwinski, J., Heeb, N., Baltensperger, U., Slowik, J. G., & Prévôt, A. S. H. (2018). Gas-phase composition and secondary organic aerosol formation from standard and particle filter-retrofitted gasoline direct injection vehicles investigated in a batch and flow reactor. *Atmospheric Chemistry and Physics, 18*(13), 9929–9954. https://doi.org/10.5194/acp-18-9929-2018

Platt, S. M., El Haddad, I., Pieber, S. M., Zardini, A. A., Suarez-Bertoa, R., Clairotte, M., Daellenbach, K. R., Huang, R.-J., Slowik, J. G., Hellebust, S., Temime-Roussel, B., Marchand, N., de Gouw, J., Jimenez, J. L., Hayes, P. L., Robinson, A. L., Baltensperger, U., Astorga, C., & Prévôt, A. S. H. (2017). Gasoline cars produce more carbonaceous particulate matter than modern filter-equipped diesel cars. *Scientific Reports, 7*(1), 4926. https://doi.org/10.1038/s41598-017-03714-9

Platt, S. M., El Haddad, I., Zardini, A. A., Clairotte, M., Astorga, C., Wolf, R., Slowik, J. G., Temime-Roussel, B., Marchand, N., Ježek, I., Drinovec, L., Močnik, G., Möhler, O., Richter, R., Barmet, P., Bianchi, F., Baltensperger, U., & Prévôt, A. S. H. (2013). Secondary organic aerosol formation from gasoline vehicle emissions in a new mobile environmental reaction chamber. *Atmospheric Chemistry and Physics, 13*(18), 9141–9158. https://doi.org/10.5194/acp-13-9141-2013

Presto, A. A., Gordon, T. D., & Robinson, A. L. (2014). Primary to secondary organic aerosol: Evolution of organic emissions from mobile combustion sources. *Atmospheric Chemistry and Physics, 14*(10), 5015–5036. https://doi.org/10.5194/acp-14-5015-2014

Roth, P., Yang, J., Peng, W., Cocker, D. R., Durbin, T. D., Asa-Awuku, A., & Karavalakis, G. (2020). Intermediate and high ethanol blends reduce secondary organic aerosol formation from gasoline direct injection vehicles. *Atmospheric Environment, 220*, Article 117064. https://doi.org/10.1016/j.atmosenv.2019.117064

Saliba, G., Saleh, R., Zhao, Y., Presto, A. A., Lambe, A. T., Frodin, B., Sardar, S., Maldonado, H., Maddox, C., May, A. A., Drozd, G. T., Goldstein, A. H., Russell, L. M., Hagen, F., & Robinson, A. L. (2017). Comparison of gasoline direct-injection (GDI) and port fuel injection (PFI) vehicle emissions: Emission certification standards, cold-start, secondary organic aerosol formation potential, and potential climate impacts. *Environmental Science and Technology, 51*(11), 6542–6552. https://doi.org/10.1021/acs.est.6b06509

Suarez-Bertoa, R., Pechout, M., Vojtíšek, M., & Astorga, C. (2020). Regulated and non-regulated emissions from Euro 6 diesel, gasoline and CNG vehicles under real-world driving conditions. *Atmosphere, 11*(2), 204. https://doi.org/10.3390/atmos11020204

Timonen, H., Karjalainen, P., Saukko, E., Saarikoski, S., Aakko-Saksa, P., Simonen, P., Murtonen, T., Dal Maso, M., Kuuluvainen, H., Bloss, M., Ahlberg, E., Svenningsson, B., Pagels, J., Brune, W. H., Keskinen, J., Worsnop, D. R., Hillamo, R., & Rönkkö, T. (2017). Influence of fuel ethanol content on primary emissions and secondary aerosol formation potential for a modern flex-fuel gasoline vehicle. *Atmospheric Chemistry and Physics, 17*(8), 5311–5329. https://doi.org/10.5194/acp-17-5311-2017

Tkacik, D. S., Lambe, A. T., Jathar, S., Li, X., Presto, A. A., Zhao, Y., Blake, D., Meinardi, S., Jayne, J. T., Croteau, P. L., & Robinson, A. L. (2014). Secondary organic aerosol formation from in-use motor vehicle emissions using a potential aerosol mass reactor. *Environmental Science and Technology, 48*(19), 11235–11242. https://doi.org/10.1021/es502239v

Virkkula, A. (2021). Modeled source apportionment of black carbon particles coated with a light-scattering shell. *Atmospheric Measurement Techniques, 14*, 3707–3719. https://doi.org/10.5194/amt-14-3707-2021

Willis, M. D., Lee, A. K. Y., Onasch, T. B., Fortner, E. C., Williams, L. R., Lambe, A. T., Worsnop, D. R., & Abbatt, J. P. D. (2014). Collection efficiency of the soot-particle aerosol mass spectrometer (SP-AMS) for internally mixed particulate black carbon. *Atmospheric Measurement Techniques, 7*(12), 4507–4516. https://doi.org/10.5194/amt-7-4507-2014

Worton, D. R., Isaacman, G., Gentner, D. R., Dallmann, T. R., Chan, A. W. H., Ruehl, C., Kirchstetter, T. W., Wilson, K. R., Harley, R. A., & Goldstein, A. H. (2014). Lubricating oil dominates primary organic aerosol emissions from motor vehicles. *Environmental Science and Technology, 48*(7), 3698–3706. https://doi.org/10.1021/es405375j

Wu, Y., Zhang, S., Hao, J., Liu, H., Wu, X., Hu, J., Walsh, M. P., Wallington, T. J., Zhang, K. M., & Stevanovic, S. (2017). On-road vehicle emissions and their control in China: A review and outlook. *The Science of the Total Environment, 574*, 332–349. https://doi.org/10.1016/j.scitotenv.2016.09.040

Yang, Z., Liu, Y., Wu, L., Martinet, S., Zhang, Y., Andre, M., & Mao, H. (2020). Real-world gaseous emission characteristics of Euro 6b light-duty gasoline- and diesel-fueled vehicles. *Transportation Research Part D: Transport and Environment, 78*, Article 102215. https://doi.org/10.1016/j.trd.2019.102215

Zhao, Y., Lambe, A. T., Saleh, R., Saliba, G., & Robinson, A. L. (2018). Secondary organic aerosol production from gasoline vehicle exhaust: Effects of engine technology, cold start, and emission certification standard. *Environmental Science and Technology, 52*(3), 1253–1261. https://doi.org/10.1021/acs.est.7b05045

Zhao, Y., Nguyen, N. T., Presto, A. A., Hennigan, C. J., May, A. A., & Robinson, A. L. (2016). Intermediate volatility organic compound emissions from on-road gasoline vehicles and small off-road gasoline engines. *Environmental Science and Technology, 50*(8), 4554–4563. https://doi.org/10.1021/acs.est.5b06247

Zhao, Y., Saleh, R., Saliba, G., Presto, A. A., Gordon, T. D., Drozd, G. T., Goldstein, A. H., Donahue, N. M., & Robinson, A. L. (2017). Reducing secondary organic aerosol formation from gasoline vehicle exhaust. *Proceedings of the National Academy of Sciences, 114*(27), 6984–6989. https://doi.org/10.1073/pnas.1620911114